Bin Liu
Department of Biomedical Engineering,
College of Engineering,
Peking University,
Zhongguancunbei Street,
The Leo KoGuan Building, Room 2-305,
Beijing 100871, China
e-mail: 1601111667@pku.edu.cn

Aoyu Zhang
Department of Biomedical Engineering,
College of Engineering,
Peking University,
Zhongguancunbei Street,
The Leo KoGuan Building, Room 2-301,
Beijing 100871, China
e-mail: 1101111324@pku.edu.cn

John Liu
Department of Mechanical Engineering,
Massachusetts Institute of Technology,
77 Massachusetts Avenue,
Building 3, Room 137,
Cambridge, MA 02139
e-mail: johnhliu@mit.edu

Zhimin Han
Department of Biomedical Engineering,
College of Engineering,
Peking University,
Zhongguancunbei Street,
The Leo KoGuan Building, Room 2-301,
Beijing 100871, China
e-mail: Jimmyhanzm@126.com

Tianyu Xie[1]
Department of Biomedical Engineering,
College of Engineering,
Peking University,
Zhongguancunbei Street,
The Leo KoGuan Building, Room 2-304,
Beijing 100871, China
e-mail: 1001111168@pku.edu.cn

Design and Evaluation of a Novel Rotatable One-Element Snake Bone for NOTES

The distal head of the natural orifice transluminal endoscopic surgery (NOTES) platform commonly uses the structure of a snake bone, which cannot rotate, and the manufacturing is often time-consuming. A novel rotatable, one-element snake bone for NOTES is proposed. This paper first describes the movement mechanism and actuation. The new structure, which is composed of hinge pairs for bending and track-sled rings for rotation, was designed to reach a 90 deg bending angle and 62 deg rotational angle. The workspace of the snake bone was derived using screw theory and was simulated on MATLAB. *The relationship between the angle and wire displacement was analyzed in detail. The new snake bone system bent and rotated by manipulating control wires that were actuated by DC motors, and its angular movements were measured by motion sensors with an angle error within ±2.6 deg. The snake bone was mounted on a flexible tube, inserted into a colonoscopy model, and navigated by motor actuation to eventually reach the cecum. The experimental results demonstrate the new snake bone's ability to travel through a natural orifice by rotating and bending, which satisfies the mobility requirement for NOTES.*
[DOI: 10.1115/1.4039592]

Keywords: snake bone, surgical instruments, mobility, workspace, screw theory

1 Introduction

Natural orifice transluminal endoscopic surgery (NOTES) developed out of a merger of endoscopy and surgery [1]. NOTES offers the advantages of avoiding external incisions and scars, reducing pain, decreasing the amount of anesthesia required, and shortening the recovery time by using natural body orifices as the primary portals of entry for surgeries [2]. The NOTES platform consists of a flexible, hollow body, which enables travel in the interior of the human body, and a distal end (head). After the distal end passes through a natural orifice, such as a transluminal opening of the stomach, vagina, bladder, or colon, and reaches the target working place in the peritoneal cavity, several therapeutic and imaging tools can be passed through the hollow conduit of the NOTES body for use during surgery [3]. The position of the therapeutic and imaging tools is set by controlling the bending movement of the distal end, the mechanical structure of which is based on a snake bone.

Recently, there has been a focus on using the snake bone as an inspiration for the NOTES structure [4], the advantages of which include flexibility, safety, dexterity, and potential for minimization [5]. Driven by steel cables [6], shape-memory alloy [7], fluidic actuation [8], or embedded servo motors [9], the snake bone mainly consists of multiple links, such as articulated joints [10,11] or spring-like structures [12]. However, these prior snake bone designs present two major limitations. First, the movement is constrained to two bending degrees-of-freedom (DOF), which yield a limited workspace that restricts the function of NOTES. The reorientation of NOTES tools of these older designs often requires the entire flexible body to be rotated by the physician. This unwieldly manipulation results in decreased ease-of-use and imprecise control and can negatively impact the health of the physician; musculoskeletal injuries are highly correlated with high surgical procedure volume [13]. Second, the fabrication process is tedious and therefore tends to have higher manufacturing costs. For example, the bending joints in the articulated distal section must be first individually machined and then assembled together

[1]Corresponding author.
Manuscript received November 18, 2017; final manuscript received January 23, 2018; published online April 18, 2018. Editor: William Durfee.

piece-by-piece using rotation pins. Furthermore, the workspace of the distal end directly impacts the accuracy of the control of the instrument's manipulations. Shen et al. [10] described the position and workspace of the distal end with the Denavit–Hartenberg convention. However, building a model using the Denavit–Hartenberg convention is complicated [14] and time-consuming, and it could have an insignificant solution. On the other hand, Weng et al. [15] designed a kinematic model for a snake-like robot using the screw theory, the derivation of which is simple; however, the resultant structure is complicated.

To overcome the drawbacks of the current designs, we propose a novel design for the snake bone that introduces an additional DOF via rotating the distal end rather than the entire body. The revised snake bone design features rotation segments that are controlled by wires that a physician can manipulate for increased control. Since the surgical tools are also installed in the snake bone structure, the rotating function increases the tool's mobility and operability. This presents the potential to decrease both the number of required tools and the overall diameter of the NOTES body. The body is machined as a single element and therefore minimizes the work of assembly. To precisely control the distal end in real time, we build the snake bone model through screw theory, which is capable of fast solutions and presents the calculations of the workspace and the relation between the control wire displacement and angle. The experimental results validated the performance of the snake bone.

2 Methods

2.1 Design Requirements. The material of the snake bone must have a certain strength to withstand the stresses created by the forces exerted on the control wires. The outer diameter of a snake bone that is capable of mounting two instrument channels should be approximately 12 mm (e.g., GIF-2TH180, OLYMPUS, Tokyo, Japan). The angle of the bending movement driven with two pairs of wires should come up to 90 deg in four directions: up, down, left, and right. To increase the workspace of the surgical instruments and decrease the manipulation of the rotation, the snake bone must add another rotational degree-of-freedom, which can be actuated by a pair of wires such that the entire range of rotational motion sums up to approximately 60 deg. The structure also consists of articulated joints, in which rivets do not fix adjacent links, and thus, the manufacturing of the snake bone is not time-consuming.

2.2 Design and Prototyping. The new snake bone design (Fig. 1) is explained in sections of movement mechanism and actuation.

2.2.1 Design of Bending and Rotation Mechanism. The rotatable one-element snake bone was machined from a single stainless steel tube 11.8 mm in outer diameter, 0.4 mm in thickness, and 125.8 mm in length. The various cuts formed hinge pairs for bending (1) and track-sled rings for rotation (2) (as shown in Fig. 1). The bending pair consists of a female hinge (3) and a male hinge (4), the rotation of which yields a bending of 15 deg per pair. Figure 2 shows the schematic diagram of bending θ between the female hinge and male hinge. To avoid segments disconnecting during bending, the square pivot (5) was introduced to both sides of the bending pair to provide stability.

The entire snake bone consists of six identical rotatable bending units (as shown in the magnified viewing area of Fig. 1), one proximal unit (6), and one distal unit (7). The rotational feature is composed of stacks of rings, 31 in total, with each ring a series of tracks (female) (8) and sleds (male) (9) around the body circumference, which yields a rotation of 2 deg per ring. Figure 3 shows the schematic diagram of rotating δ between the track and sled. To avoid risking the disconnection of segments during rotation, the number of track-sled pairs around a ring was increased, thereby decreasing the slippage between segments.

The angular displacements of each of the hinge pairs and track-sled rings sum to a designed total of 90 deg of body bending angle and 62 deg of body rotation angle, respectively.

2.2.2 Analysis. The workspace of snake-like bone was modeled using screw theory. We first introduce the bending movement

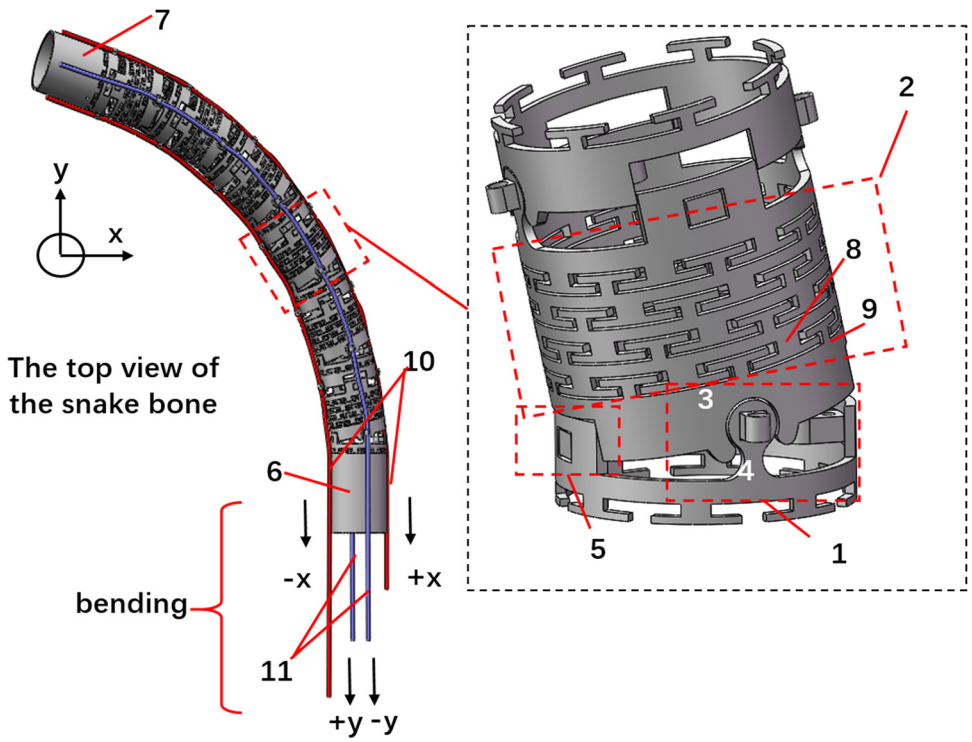

Fig. 1 The design of the rotatable one-element snake bone: one segment consists of pairs of bending hinges and a rotational section of track-sled rings

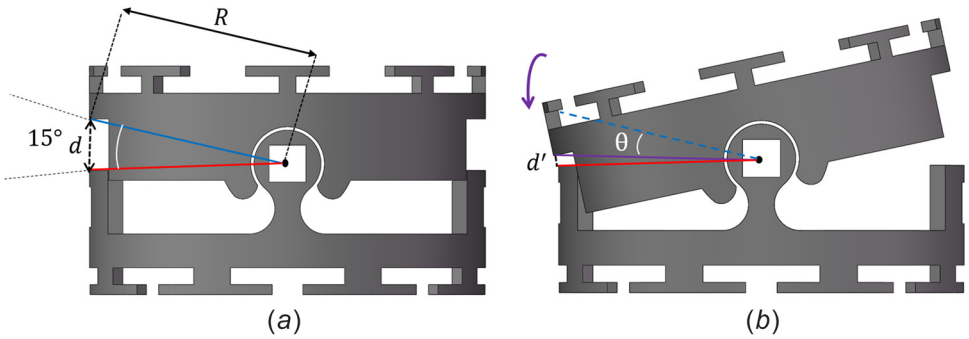

Fig. 2 Schematic diagram of the bending angle θ between the female hinge and male hinge: (*a*) original and (*b*) bending θ status of the adjacent links

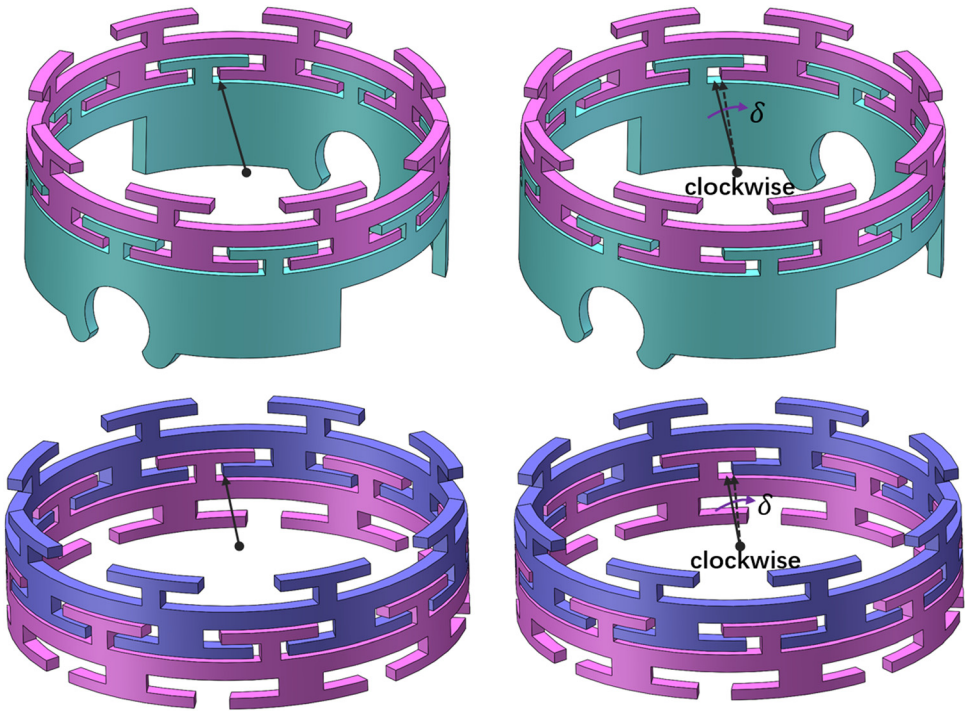

Fig. 3 Schematic diagram of the rotating angle δ between the track and sled

of hinge pairs. According to screw theory, if$g(0)$ represents the initial configuration of the tip of the female hinge with respect to coordinate S, then the final configuration generated by rotating about a fixed axis with respect to the same coordinate S is given by

$$g(\theta) = e^{\hat{\xi}\theta} g(0) \tag{1}$$

$$e^{\hat{\xi}\theta} = \begin{bmatrix} e^{\hat{\omega}\theta} & (I - e^{\hat{\omega}\theta})(\omega \times v) + \omega\omega^T v\theta) \\ 0 & 1 \end{bmatrix}, \quad \omega \neq 0 \tag{2}$$

In Eq. (1), $e^{\hat{\xi}\theta}$ is a mapping from the initial position $g(0)$ to the next position $g(\theta)$ after rotating by an angle θ. In Eq. (2), $e^{\hat{\omega}\theta} = I + \hat{\omega}\sin\theta + \hat{\omega}^2(1 - \cos\theta)$, $\omega \in R^3$, $\|\omega\| = 1$, is the axis of rotation; θ is the angle of rotation; and $v = -\omega \times q$, $q \in R^3$ is a point on the axis. Note that $\hat{\omega}$ can be calculated using the following formula:

$$\hat{\omega} = \begin{bmatrix} 0 & -\omega_3 & \omega_2 \\ \omega_3 & 0 & -\omega_1 \\ -\omega_2 & \omega_1 & 0 \end{bmatrix}, \quad \text{if } \omega = (\omega_1; \omega_2; \omega_3) \tag{3}$$

By using Eqs. (1)–(3), we can obtain the final position of the tip of the female hinge, after it has bent a certain angle θ about the axis located in the center of the articulated joints between the female hinge and male hinge.

This paper assumes that the center of the base of the snake bone is the origin of the reference coordinate system. As mentioned earlier, the snake bone is composed of six rotatable bending units, and thus, the final position of the tip of the snake bone (TSB) can be found by

$$g_{st}(\theta) = e^{\hat{\xi}_1\theta} e^{\hat{\xi}_2\theta} e^{\hat{\xi}_3\theta} e^{\hat{\xi}_4\theta} e^{\hat{\xi}_5\theta} e^{\hat{\xi}_6\theta} g_{st}(0) \tag{4}$$

where each pair of hinges bends to an angle θ in one direction without rotation, and $g_{st}(0)$ is the initial position of TSB.

The calculation is similar in other orthogonal directions. The values of ω that are parallel to the y-axis for six articulated joints are $[0; 1; 0]$, i.e., the orthogonal six axes parallel with the x-axis are $[1; 0; 0]$.

Table 1 lists the values of $g_{st}(0)$ and q, points on the six axes parallel with the y-axis.

Using Eqs. (1)–(4), when each bending pair yields a bend of 15 deg, the final coordinate $g_{st}(\theta)$ of the TSB is [78.8852, 0, 73.0852] relative to the reference coordinate system. To calculate the angle of bending, α, another final position, $g_{st'}(\theta)$, of point

Table 1 Points on the six axes parallel to the *y*-axis

Points	x	y	z
$g_{st}(0)$	0	0	125.8
q_1	0	0	19.0
q_2	0	0	35.4
q_3	0	0	51.8
q_4	0	0	68.2
q_5	0	0	84.6
q_6	0	0	101.0

$g_{st'}(0)$ (i.e., [0, 0, 110]) below the tip must be calculated with the same method. The angle can be found through the law of cosines

$$\cos\alpha = \frac{(g_{st}(\theta) - g_{st'}(\theta)) \cdot k}{|g_{st}(\theta) - g_{st'}(\theta)| \cdot |k|} \tag{5}$$

where k is the unit vector in the z positive direction; then, $\alpha = 90$. Thus, the maximum angle of bending meets the design requirement.

Next, adding another DOF of bending to the y direction, with $\omega = [1; 0; 0]$, the final position of the tip can be obtained as follows:

$$g_{st}(\theta) = e^{\hat{\xi}_{y1}\theta_x} e^{\hat{\xi}_{x1}\theta_y} e^{\hat{\xi}_{y2}\theta_x} e^{\hat{\xi}_{x2}\theta_y} e^{\hat{\xi}_{y3}\theta_x} e^{\hat{\xi}_{x3}\theta_y} e^{\hat{\xi}_{y4}\theta_x} e^{\hat{\xi}_{x4}\theta_y} e^{\hat{\xi}_{y5}\theta_x} e^{\hat{\xi}_{x5}\theta_y} e^{\hat{\xi}_{y6}\theta_x} e^{\hat{\xi}_{x6}\theta_y} g_{st}(0) \tag{6}$$

where $e^{\hat{\xi}_{yi}\theta_x}$ and $e^{\hat{\xi}_{xi}\theta_y}(i = 1, 2, 3, 4, 5, 6)$ are, respectively, the exponential of twist about the six axes parallel with the y-axis and x-axis; θ_x and θ_y are the bending angles of each of the hinge pairs toward the x- and y-directions, respectively.

To simulate the real position of TSB, the rotation of stacks of rings, composed of tracks (female) (8) and sleds (male) (9), must be added. As mentioned above, 31 rings form the rotatable feature, and thus, the final formula after derivation is shown in the following equation:

$$\begin{aligned} g_{st}(\theta) = {} & e^{\hat{\xi}_{z1}\delta} e^{\hat{\xi}_{y1}\theta_x} \left(\prod_{i=2}^{5} e^{\hat{\xi}_{zi}\delta} \right) e^{\hat{\xi}_{x1}\theta_y} e^{\hat{\xi}_{z6}\delta} e^{\hat{\xi}_{y2}\theta_x} \\ & \left(\prod_{i=7}^{10} e^{\hat{\xi}_{zi}\delta} \right) e^{\hat{\xi}_{x2}\theta_y} e^{\hat{\xi}_{z11}\delta} e^{\hat{\xi}_{y3}\theta_x} \left(\prod_{i=12}^{15} e^{\hat{\xi}_{zi}\delta} \right) e^{\hat{\xi}_{x3}\theta_y} e^{\hat{\xi}_{z16}\delta} e^{\hat{\xi}_{y4}\theta_x} \\ & \left(\prod_{i=17}^{20} e^{\hat{\xi}_{zi}\delta} \right) e^{\hat{\xi}_{x4}\theta_y} e^{\hat{\xi}_{z21}\delta} e^{\hat{\xi}_{y5}\theta_x} \left(\prod_{i=22}^{25} e^{\hat{\xi}_{zi}\delta} \right) e^{\hat{\xi}_{x5}\theta_y} e^{\hat{\xi}_{z26}\delta} e^{\hat{\xi}_{y6}\theta_x} \\ & \left(\prod_{i=27}^{30} e^{\hat{\xi}_{zi}\delta} \right) e^{\hat{\xi}_{x6}\theta_y} e^{\hat{\xi}_{z31}\delta} g_{st}(0) \end{aligned} \tag{7}$$

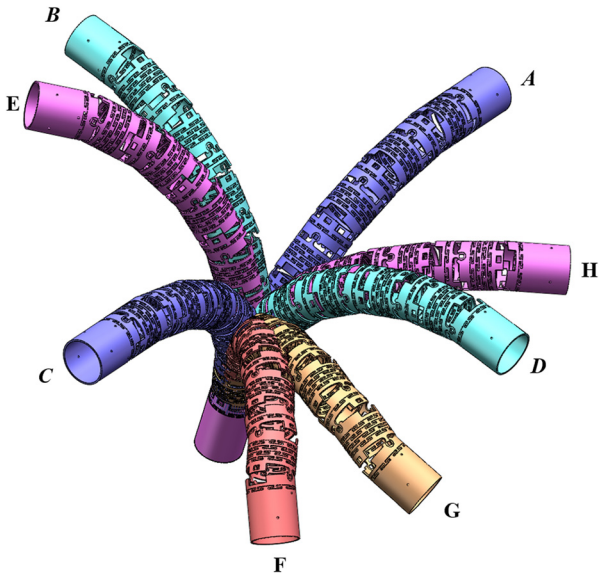

Fig. 5 Some extreme gestures: certain angle or multiple angles reach the maximum

Table 2 Implication of letters (rcc, rotate counterclockwise)

Symbol	Meaning	Symbol	Meaning
A	$x + 90$ deg	E	$y + 90$ deg, rcc 62 deg
B	$y + 90$ deg	F	$x - 90$ deg, $y - 90$ deg
C	$x - 90$ deg	G	$x - 90$ deg, $y - 90$ deg, rcc 62 deg
D	$y - 90$ deg	H	$y - 90$ deg, rcc 62 deg

Here, δ is the angle of each ring that is rotating about the central axis of the ring, and $e^{\hat{\xi}_{zi}\delta}(i = 1, 2, \ldots, 31)$ are the exponentials of the twist about the 31 axes parallel to the z-axis. Using Eq. (7), the coordinate of TSB can be found, and the workspace of the snake bone with rotation can also be calculated by adjusting the values of the parameters $(\theta_x, \theta_y, \delta)$. MATLAB was used to simulate the workspace, and the results are shown in Fig. 4. Some extreme gestures, with certain angles or multiple angles reaching the maximum, are shown in Fig. 5, and Table 2 gives the specifics of each position.

Compared with a workspace that does not employ rotation, the situation with respect to rotation is appreciable, and thus, it

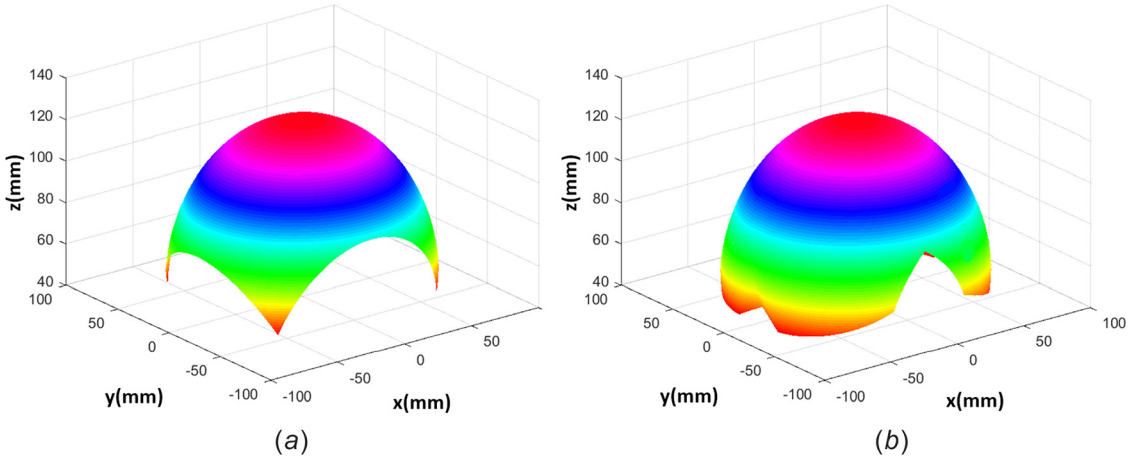

Fig. 4 Workspace of the revised snake bone: results generated by: (*a*) adjusting θ_x, θ_y without rotation and (*b*) adjusting θ_x, θ_y, and δ

demonstrates that this new design of snake bone can significantly improve the mobility of surgical instruments.

2.2.3 Design of Actuation Mechanisms. Two pairs of wires (10) and (11) were threaded through small guide tubes that were positioned along the external wall of the body (Fig. 1). Bending is achieved through pulling and releasing these bending wires. Bending θ between the female hinge and male hinge, and wire displacement (Fig. 2) along with the body, can be found in Eq. (8). Multiplying Δd_{bw} by six, the total wire displacement for one wire can be obtained

$$\Delta d_{\text{bw}} = d - d' = 2R\sin\left(\frac{15\,\text{deg}}{2}\right) - 2R\sin\left(\frac{15\,\text{deg}}{2} - \frac{\theta}{2}\right) \quad (8)$$

where $R(5.95\,\text{mm})$ is the bending radius.

The rotation wires (12) were threaded through small guide tubes that were positioned along the internal wall of the body to form a helix with variable pitch (Fig. 6(*a*)). At the bottom of the snake bone, the pair of wires begins parallel to the axis to promote smooth pulling. The pair of wires spiral up the body axis to form a helix of decreasing pitch toward the top of the snake bone, which yields increasing force for rotation and smaller sliding friction as the helix approaches the top. To calculate the relation between the rotation angle and rotation wire displacement, we unfolded the snake bone structure from the upper fixed point P to the lower wire outlet, as shown in Fig. 6(*b*). Pulling and releasing these rotation wires rotates the entire body, which makes point P move to point P'. The rotational distance Δd_r and rotation wire displacement Δd_{rw} are obtained as follows:

$$\Delta d_r = \varphi r \quad (9)$$

$$\Delta d_{rw} = \sqrt{L^2 + h^2} - \sqrt{(L - \Delta d_r)^2 + h^2} \quad (10)$$

where φ ($\varphi = 31 \cdot \delta$) is the total angle (radians) of a counterclockwise rotation about the central axis of the body; $r(5.90\,\text{mm})$ is the body radius; $L(L = 3.5\pi r)$ is 3.5 times half the perimeter of the body undersurface; $h(80\,\text{mm})$ is the height between the upper fixed point and the wire outlet. Figure 7 shows the relation between the rotation wire displacement and the rotation angle.

The relationship between the wire displacement and the bending or rotational angle is essentially linear (Eq. (8) and Fig. 7). Thus, according to Eqs. (5)–(10), the position and angle situation of TSB can be estimated by measurement of the wire displacement.

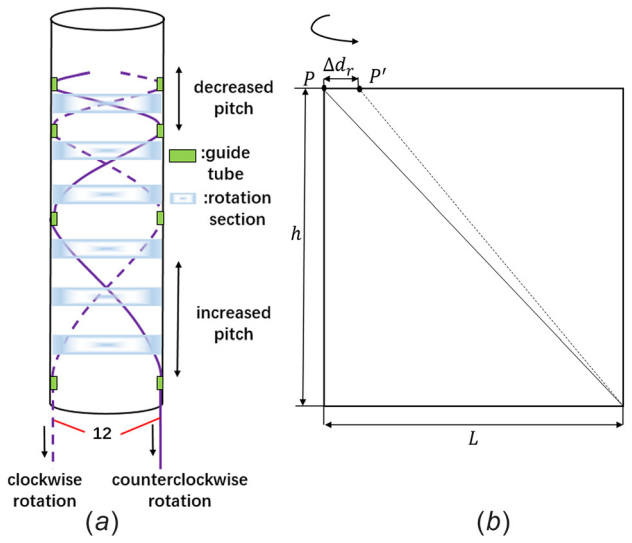

Fig. 6 The rotational actuation of the snake bone: a pair of wires spiral up the body axis to form a helix of decreasing pitch toward the top of the snake bone

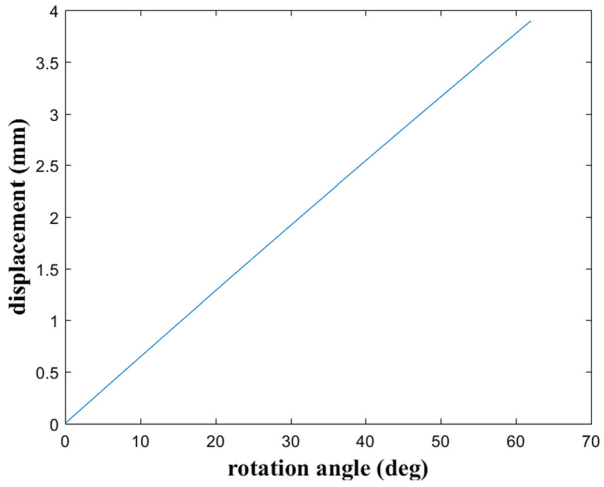

Fig. 7 The relation between the rotation wire displacement and rotation angle

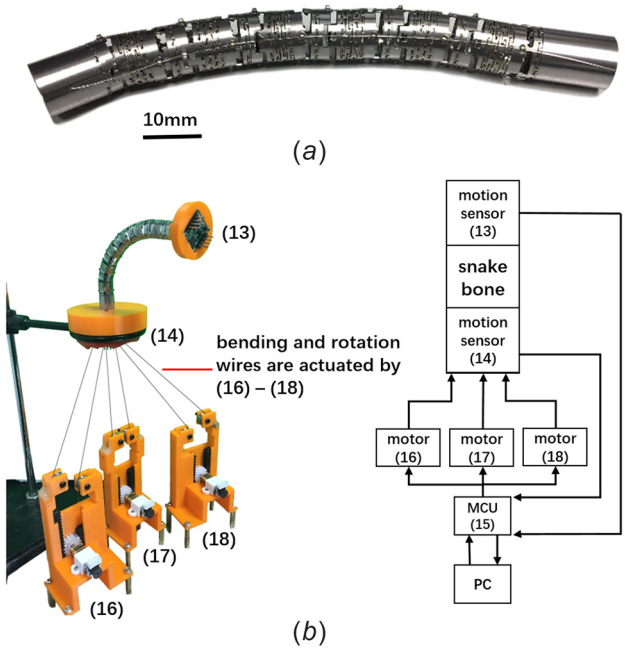

Fig. 8 Fabrication and validation: (*a*) the machined snake bone is laser machined as one piece and (*b*) the experimental setup and schematic

2.3 Fabrication of the Control System. The snake bone was machined by a laser cutter (StarCut Tube, Rofin Co., Ltd., Hamburg, Germany), and the guide tubes were glued into the body structure (Fig. 8(*a*)). Two motion sensors (MPU-9250, InvenSense, Inc., San Jose, CA) ((13) and (14) in Fig. 8(*b*)) were attached onto the distal end and proximal end of the snake bone (Fig. 8(*b*)). The bending angle and the rotation angle were defined as the difference between the corresponding angles of the two motion sensors. The angular data were collected by a microcontroller unit (STM32F103ET, ST CO., Ltd., Agrate Brianza and Catania & Tours, Italy & France) ((15) in Fig. 8(*b*)). The angle and rotation wires were actuated by three DC motors (GM12-N20K, TT Motor (HK) Industrial Co., Ltd., Hong Kong, China) ((16)–(18) in Fig. 8(*b*)) under the control of a microcontroller

unit. To improve on the previous system that used fish wire for its control wires [16], steel wire was used instead, which thereby decreased the elasticity and increased the precision of control.

3 Results

Four experiments were performed to evaluate the function of the new snake bone design. The first experiment examined the rotation of the snake bone bent at three different angles: 0, 30, and 60 deg. The second experiment examined the bending of the snake bone without rotation to ensure the alignment of the guide tubes. The pulling of the control wires was kept at a constant 7 mm/s and reached its maximum displacements in the first and second experiments, at 3.9 mm and 9.3 mm, respectively. Each experiment consisted of 100 trials, the averages of which are shown as single profiles (Fig. 9).

The snake bone rotated up to 62 deg for 0 deg of bending (Fig. 9(*a*)). Increasing the bending angle changed the shape of the rotation wires and increased the frictional forces that the wire experienced, thus increasing the wire displacement that was required for the same resultant body rotation. The bending profile (Fig. 9(*b*)) demonstrates the bending function of the snake bone. The bending angle increased along with the wire displacement, and the averages over 100 trials are shown. These curves are different from prior work [16] because the steel wires of the new design experienced little extension during the trials.

The third experiment tested the deflection angles (DA) between the TSB and the unit vector in the z positive direction (as shown in Fig. 10) at certain values of the bending and rotational angles, to examine the reliability of the design. Here, η ($\eta = 6 \cdot \theta_x$),ϕ($\phi = 6 \cdot \theta_y$) represent the total bending angle toward the x positive direction and the y positive direction, respectively. Table 3 compares the DA as simulated using MATLAB and experimentally measured. The results demonstrate the stability of the control system and its potential for precise control in surgical instruments.

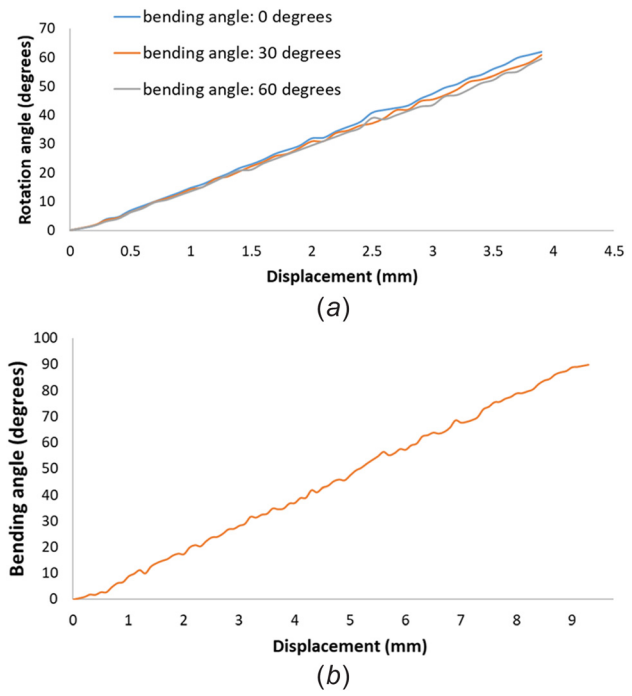

Fig. 9 Bending and rotation as a function of the pulled wire displacement. The average of 100 trials is presented as a single profile. For clarity, bending and rotation in only one direction is displayed. The maximum body bending angle and body rotation angle is 90 and 62 deg, respectively.

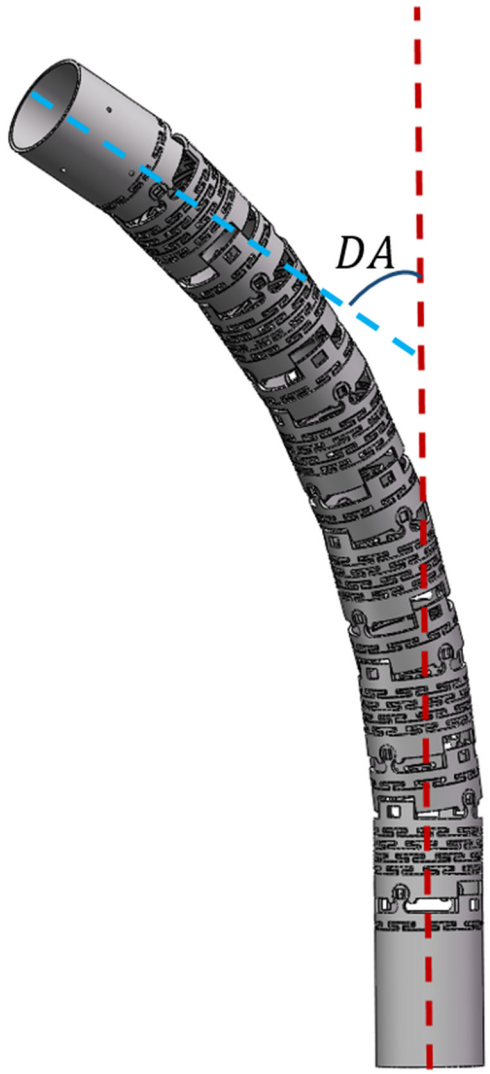

Fig. 10 Deflection angles between the TSB and unit vector in the *z* positive direction

Table 3 Simulated and actual measurement in some specific configurations

η (deg)	ϕ (deg)	φ (deg)	DA (deg) (simulating)	DA (deg) (real, 120 trials)
45	0	0	45	45±1.54
0	45	0	45	45±1.63
45	45	0	63.54	63.5±1.42
90	90	0	126.11	126±1.87
0	45	31	44.47	44±2.28
0	90	62	84.89	84±2.42
90	0	62	84.89	85±2.06
45	45	31	66.37	66±1.97
90	90	62	105.71	105±2.51

In the last experiment, we assembled an inserted instrument and simulated the use case. The instrument was composed of the new snake bone, a hollow flexible tube, and a camera (Fig. 11). A snake bone was mounted on one end of the tube, and a small universal serial bus camera was passed through the entire hollow body to take photos. The protective rubber sleeve, which featured a smooth inner surface, was wrapped around the snake bone. This instrument was inserted into a colonoscopy training model (Colonoscopy Training Model I-B, Koken Co., Ltd., Tokyo, Japan). By controlling the motions of the motors to rotate and bend the distal

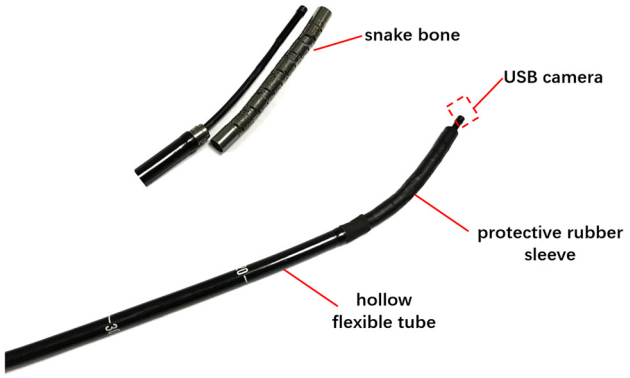

Fig. 11 Illustration of the inserted instrument

end, the device traveled in the interior of the model and took pictures at specific locations of the model (Fig. 12), eventually reaching the cecum. The result of this test case demonstrates the device's ability to travel in a natural orifice through rotation and bending.

4 Conclusions

In this paper, we have presented the design, fabrication, and experimental validation and characterization of a novel snake bone for NOTES with the movements of both rotation and bending. The one-element snake bone for NOTES has several advantages over the traditional design. First, the surgical instruments installed inside the hollow snake bone can rotate 62 deg about the central axis of the body, which is actuated by the rotation wires, which decreases the wrist load and subsequently increases the ease-of-use for the physician. At the same time, the design of the snake bone significantly increases the workspace and mobility of the surgical instruments. These advantages demonstrate the importance of introducing a rotational DOF into the snake bone design.

Second, the manufacturing of the new snake bone design requires substantially less fabrication time and less human labor. The body of this new snake bone can be machined as one piece using a laser-cutting machine, which obviates the need for manual assembly and, thus, presents the potential for mass production.

This work also found the relation between the wire displacement and the bending or rotational angle, which furthers the precision of the manipulation. The bending and rotation functionality of the prototype was tested using a setup of motion sensors and actuators in the paper. These validated results present the potential that this design can satisfy the requirements for NOTES. Future work will entail the design of rotation-agnostic bending, the integration of the snake bone into the NOTES platform, and in vivo testing.

References

[1] Kalloo, A. N., Singh, V. K., Jagannath, S. B., Niiyama, H., and Hill, S. L., 2004, "Flexible Transgastric Peritoneoscopy: A Novel Approach to Diagnostic and Therapeutic Interventions in the Peritoneal Cavity," Gastrointest. Endosc., **60**(1), pp. 114–117.
[2] Zhou, Y., Ren, H., Meng, M. Q.-H., Tse, Z. T. H., and Yu, H., 2013, "Robotics in Natural Orifice Transluminal Endoscopic Surgery," J. Mech. Med. Biol., **13**(2), p. 1350044.
[3] Mummadi, R. R., and Pasricha, P. J., 2008, "The Eagle or the Snake: Platforms for NOTES and Radical Endoscopic Therapy," Gastrointest. Endosc. Clin. N. Am., **18**(2), pp. 279–289.
[4] Pourghodrat, A., Nelson, C. A., and Oleynikov, D., 2017, "Hydraulic Robotic Surgical Tool Changing Manipulator," ASME J. Med. Devices, **11**(1), p. 011008.
[5] Kim, Y.-J., Cheng, S., Kim, S., and Iagnemma, K., 2014, "A Stiffness-Adjustable Hyperredundant Manipulator Using a Variable Neutral-Line Mechanism for Minimally Invasive Surgery," IEEE Trans. Rob., **30**(2), pp. 382–395.
[6] Li, Z., and Du, R., 2013, "Design and Analysis of a Bio-Inspired Wire-Driven Multi-Section Flexible Robot," Int. J. Adv. Rob. Syst., **10**(4), p. 209.
[7] Ayvali, E., Liang, C. P., Ho, M., Chen, Y., and Desai, J. P., 2012, "Towards a Discretely Actuated Steerable Cannula for Diagnostic and Therapeutic Procedures," Int. J. Rob. Res., **31**(5), pp. 588–603.
[8] Devreker, A., Rosa, B., Desjardins, A., Alles, E. J., and Garcia-Peraza, L. C., 2015, "Fluidic Actuation for Intra-Operative In Situ Imaging," IEEE/RSJ International Conference on Intelligent Robots and Systems (IROS), Hamburg, Germany, Sept. 28–Oct. 2, pp. 1415–1421.
[9] Son, J., Cho, C. N., Kim, K. G., Chang, T. Y., Jung, H., Kim, S. C., Kim, M. T., Yang, N., Kim, T. Y., and Sohn, D. K., 2015, "A Novel Semi-Automatic Snake Robot for Natural Orifice Transluminal Endoscopic Surgery: Preclinical Tests in Animal and Human Cadaver Models (With Video)," Surg. Endosc., **29**(6), pp. 1643–1647.
[10] Shen, T., Nelson, C. A., Warburton, K., and Oleynikov, D., 2015, "Design and Analysis of a Novel Articulated Drive Mechanism for Multifunctional NOTES Robot," ASME J. Mech. Rob., **7**(1), p. 011004.

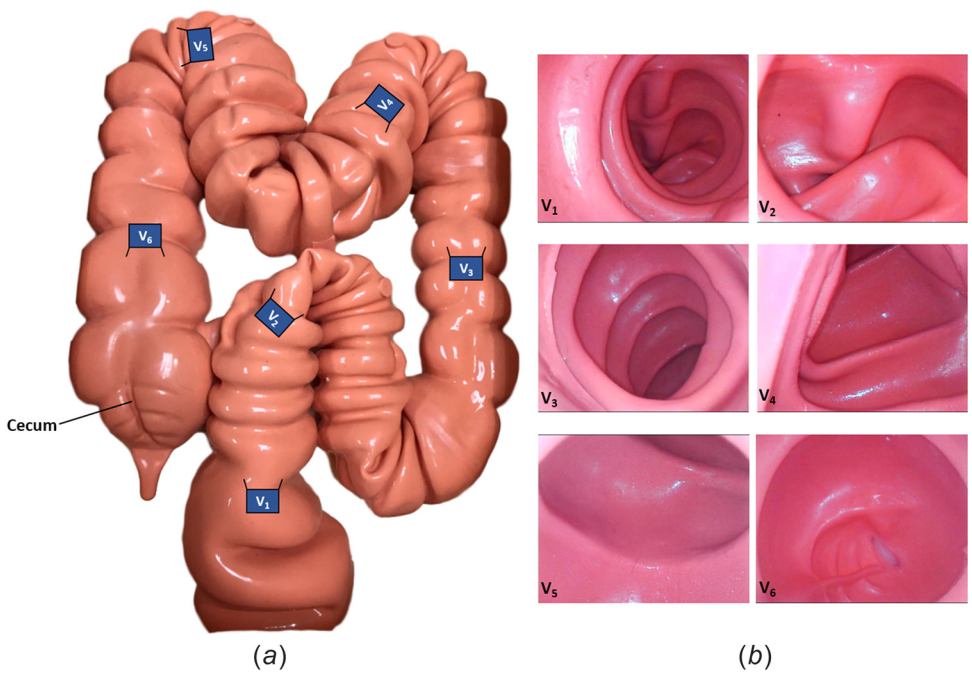

Fig. 12 Colonoscopy training model and some pictures at specific locations in the model. V_1–V_6 represents the location of the camera.

[11] Patel, N., Seneci, C. A., Shang, J., Leibrandt, K., Yang, G. Z., Darzi, A., and Teare, J., 2015, "Evaluation of a Novel Flexible Snake Robot for Endoluminal Surgery," Surg. Endosc., **29**(11), pp. 3349–3355.
[12] Tan, Z., and Ren, H., 2014, "Design and Actuation of a Snake-like Robot for Minimally Invasive Surgeries," 15th International Conference on Biomedical Engineering, Singapore, Dec. 4–7, pp. 28–31.
[13] Harvin, G., 2014, "Review of Musculoskeletal Injuries and Prevention in the Endoscopy Practitioner," J. Clin. Gastroenterol., **48**(7), pp. 590–594.
[14] Richard, M., Murray, Z. L., and Shankar Sastry, S., 1994, *A Mathematical Introduction to Robotic Manipulation*, CRC Press, Boca Raton, FL.
[15] Weng, Z., Liu, T., Wu, C., and Cao, Z., 2016, "Mechanism Design and Kinematic Performance Research of Snake-Like Robot With Orthogonal Active Wheels," *Advances in Reconfigurable Mechanisms and Robots II* (Mechanisms and Machine Science), Springer, Cham, Switzerland, pp. 603–615.
[16] Zhang, A., Liu, B., Liu, J., and Xie, T., 2017, "Design of a Rotatable One-Element Snake Bone for NOTES," ASME Paper No. DMD2017-3410.